

# Modelling of electronic and optical properties of $\text{Cu}_2\text{SnS}_3$ quantum dots for optoelectronics applications

M. IRSHAD AHAMED<sup>1,\*</sup>, K. SATHISH KUMAR<sup>2</sup>

<sup>1</sup>Department of Electronics and Communication Engineering, E.G.S. Pillay Engineering College, Nagapattinam-611002, Tamilnadu, India

<sup>2</sup>Department of Chemical Engineering, SSN College of Engineering, Kalavakkam-603110, Tamilnadu, India

Copper tin sulfide ( $\text{Cu}_2\text{SnS}_3$ ) is a unique semiconductor, whose nanocrystals have attracted researchers' attention for its tunable energy bandgap and wavelength in visible and near infrared range. Quantum dots which are fabricated from this material are highly suitable for optoelectronics and solar cell applications. This paper discusses the tunable energy bandgap, exciton Bohr radius and wavelength range of wurtzite structure of  $\text{Cu}_2\text{SnS}_3$  quantum dots to assess the opportunity to use them in optoelectronics applications. The considerations show that the mole fraction of copper increases as energy bandgap decreases and tunable energy bandgap of this quantum dot material is inversely proportional to the wavelength.

Keywords:  $\text{Cu}_2\text{SnS}_3$ ; quantum dots; tunable wavelength; bandgap; optoelectronics

## 1. Introduction

Semiconductor nanocrystals frequently referred to as quantum dots (QDs), are made by creating an island of conductive material encapsulated by an insulated material. The electron movement is highly confined in such structures and the encapsulated electron needs high potential to escape. Due to size dependent optical properties the bandgap changes in the nanoregime. As the bandgap changes, the size of QDs also changes, and simultaneously wavelength is also varied. Quantum effects play a major role in QDs, which is important and the QDs behave like an atom. If the radius of QDs is higher than exciton Bohr radius of bulk material, the quantum effects will not be dominant as mentioned before. The uniqueness of QDs is the tunable bandgap and high absorption of light which is important as it leads to photocurrent [1–3]. QDs are used for the preparation of sensors with multidimensional response signals and narrow band luminescent emission and they offer high resistance to photodegradation. They have found delicate applications in various optoelectronic devices

such as light emitting diodes (LEDs), laser diodes (LDs) [4–6], photovoltaics [2, 7, 8] and photodiodes (PDs) [9–11].

Quantum confinement plays a dominant role in theoretical calculations of QDs with respect to confinement energies, Bohr radius, wavelength etc. It is commonly accepted that if the diameter of QDs is smaller than exciton Bohr radius, the degree of movement for charge particle can be reduced from  $N$  to zero. Hence, energy levels can be calculated by using a particle in a box model in which energy level of different states depends on the length of the box. If the QD radius of nanomaterial is less than exciton Bohr radius, then the QDs are in a strong confinement regime. If the radius of nanomaterial is higher than the exciton Bohr radius then the QDs are in a weak confinement regime. Due to this quantum confinement effect, the quantum dots differ in optoelectronic properties, high emission, narrow spectral bands and tunable emission [12–15]. Further, QDs also have a large quantum yield, i.e. the percentage level of absorbed photons is higher than that of emitted photons, which is very useful in optoelectronic applications and solar cells.

QDs have size dependent bandgap, which causes that absorption and emission spectra are

\*E-mail: irshad\_bcet@yahoo.co.in

changed. By controlling the bandgap of QDs by mole fraction of the base element (Cu), their absorption and emission spectra can be controlled efficiently which is used in various applications. Larger QDs possess lesser amount of bandgap energy which results in absorption of light with longer wavelengths, similarly smaller quantum dots have larger bandgap energy with shorter wavelengths [16].

Generally, in semiconductor materials, charge carriers may have many energy levels. These energy levels are close to each other, so that it is called an energy band as shown in Fig. 1. All carriers tend to occupy the energy levels below the bandgap (i.e. in the valence band) and above the bandgap a small number of carriers are present in the conduction band. The carriers can move to the conduction band by acquiring energy supplied to the material in a form of heat, electric field potential, etc. and they leave holes in the valence band. Such electron hole pair known as exciton is important for the size of QDs [17].

Amongst different types of QDs, Cu–Sn–S QDs are most attractive for fundamental investigation and practical applications in optoelectronics and solar cells because of their high surface to volume ratio and unusual electronic and optical properties. Among different combinations of Cu–Sn–S based QDs,  $\text{Cu}_2\text{SnS}_3$  quantum dots are predominant since the phase bandgap ranges from 0.93 eV to 1.51 eV [18]. This is the most frequently studied phase in optoelectronics applications. In this research,  $\text{Cu}_2\text{SnS}_3$  QDs have been chosen for studying the changes in bandgap, wavelength and exciton Bohr radius.

### 1.1. Optoelectronic devices with wavelength converter

Nowadays, an optical wavelength converter is one of important devices in telecommunication networks [19] and sensing applications [20, 27]. It is an optoelectronic device that converts information from one wavelength to another. In fiber optic communication, wavelength division multiplexing scheme (WDM) is mostly preferred. In optoelectronics, WDM device wavelength converter

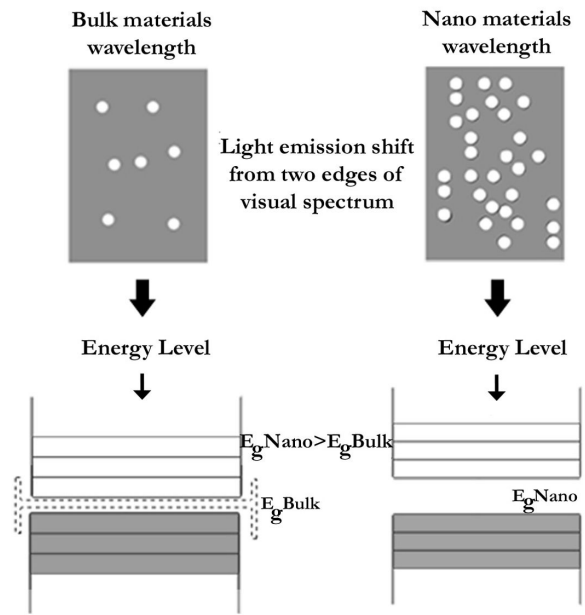


Fig. 1. Energy band diagram of bulk and nanomaterial

plays a vital role in signal processing. An important function of the wavelength converter is to avoid wavelength blocking in optical cross connecting and provide switching protection. The converter allows simpler network reconfiguration, i.e. it enables wavelength paths to be allocated in a link by link process [21].

Wavelength conversion process is roughly classified into two types, such as optoelectronic wavelength conversion and all optical wavelength conversion. In the first method of the wavelength conversion, an optical signal is converted into an electronic signal by using photodetector, then the electronic signal is stored in a buffer amplifier, further the electronic signal is passed to a tunable laser by first in first out (FIFO) queue mechanism. The tunable laser does the work to achieve a desired wavelength (Fig. 2). This method has the bit rate up to 10 Gb/s. This is a basic method of wavelength conversion, however, it is quite complex, has limited digital transparency and consumes large power for processing [22].

The second method “all optical wavelength conversion” is most commercialized and much appreciated by researchers because of its high transparency and low switching power. Semiconductor



Fig. 2. Schematic diagram of optoelectronic wavelength conversion.

optical amplifiers (SOAs) are specifically suitable for such kind of signal processing because they are featured by fast nonlinearities. In addition, they offer possibility of integration with other components in a small space [23]. Wavelength conversion process is realized through two modulation schemes: namely cross phase modulation (XPM) and cross gain modulation (XGM), for which the XGM based on SOAs gives the bit rates up to 40 Gb/s for eye diagram quality measurements [24], 80 Gb/s for multicast conversion [25] and 160 Gb/s reported in [26] while the XPM based on SOAs is commonly used as offset filtering up to 40 Gb/s for optical filtering scheme in WDM [23].

### 1.1.1. Sensors

In general, sensor is a device or subsystem or module whose purpose is to detect and respond to some types of physical inputs; the input could be light, pressure, moisture, motion or heat. The maximum output signal should be in electronic form for further processing. Thus, a sensor is always used with other electronics, either simple as light or complex as digital systems. The basic elements of sensors consist of an electronic interface and sensing element. The sensing element is used to convert one form of data (non-electrical form) into electrical form, so it can act as a transducer. Sensor head consists of sensing elements and integrated circuitry with protected casing. The whole circuit can detect even minor variation which can be recorded and transferred (for example nondispersive infrared sensor head is used for gas sensing applications). The sensing device consists of a proper sensor head with essential mechanical and electrical interfaces, but it may contain also supplementary units for further data processing and digital communication. Table 1 reports the technology

readiness level (TRL) of sensor components such as, sensing device, sensor, transducer and sensor head [19].

## 1.2. Possible applications of quantum dots

In this chapter, applications of QDs in optoelectronic devices will be discussed. The uniqueness of QDs is quantum effects in all directions in three-dimensional space. Hence, many QDs are located in semiconductor substrate in active regions of optoelectronic devices such as sensors, light emitting devices (lasers and LEDs) and semiconductor optical amplifiers (SOAs) for fiber optic communication [28].

To overcome the limitations of conventional bulk and quantum well semiconductors, optical amplifiers (SOAs), QD-SOAs have been developed. They exhibit extremely attractive features over a large bandwidth and gain, improved output saturation power and ultrafast recovery time. These fascinating features have led to the development of highly efficient and high speed optical processing intensity modulation [29]. Further, fiber to the home (FTH) requirements are rapidly increasing due to the need for high bandwidth applications. Gigabit passive optical network (GPON) is a promising technology to access the fiber optic systems. Conventional SOAs offer physical reach of 20 km between a hub and customer with a split ratio of 1:32 and a loss budget of 28 dB. However, QD-SOAs can reach 60 km between the main hub and customer with a split ratio of 1:32 and a loss budget of 45 dB. QD-SOAs combine the advantages of GPON extender solutions to reduce single chip cost effectively. They exhibit ultrafast gain response ( $\sim 1$  ps), high gain bandwidth ( $\sim 120$  nm), possibility of operation without cooling, high burst mode tolerance and insensitive operation [19]. The stability of QDs wavelength converter can be highly improved without losing its luminescent intensity [30].

Display applications in which QD materials show uniqueness in performance and composition are employed in the backlit LEDs and Liquid Crystal Displays (LCDs). Nowadays, LEDs are an essential backlight source for televisions, mobile

Table 1. Assumed technology readiness level (TRL) of sensing device and its components according to the United States “Department of Defense (DoD)” definitions.

Component or subsystem or module	Minimum TRL	Expected TRL
Transducer (sensing element)	Basics principles observed and reported (TRL 1)	“Flight proven” through successful mission operations (TRL 9)
Sensor head	Component validation in relevant environment (TRL 4)	System prototype demonstration in an operational environment (TRL 7)
Sensor	Basics principles observed and reported (TRL 1)	Component validation in relevant environment (TRL 5)
Sensing device	Subsystem model of prototype demonstration in a relevant environment (TRL 6)	Actual system proven through successful mission operations (TRL 9)

phones, laptops, tablets and most of monitors [31]. The advantage of QDs material is that it can be used as down conversion material for LCDs. Numerous prominent analyses are now forecasting next generation displays that have wide color gamut displays which can be QD-enabled [32]. Based on National Television System Committee (NTSC) Standard for color gamut, QD enabled backlit LEDs and LCDs can exhibit significantly higher efficiency, when compared with conventional LEDs and LCDs which have typically less than 70 percent efficiency [31]. Similarly tunable QD enhanced PDs operating both in infrared and visible ranges offer potentially higher response time and extraordinary sensitivities up to  $1 \times 10^{13}$  Jones [9]. There is plenty of room for the applications of QDs including low dark current and high sensitivity infrared photodetectors produced using QDs with strong carrier confinement.

## 2. Theoretical framework

The energy bandgap of QDs depends on effective mass of excited electrons, holes and dimensions of a material. In  $\text{Cu}_2\text{SnS}_3$  QDs, the energy bandgap depends on mole fraction of constituent element Cu. Absorption of wavelength can be found from the relationship between energy and wavelength  $E = hc/\lambda$ .

In this work, an attempt has been made to observe how the mole fraction and Brus equation can be used to tune the bandgap and wavelength of this ternary alloy.

### 2.1. Bandgap of $\text{Cu}_2\text{SnS}_3$ as a function of mole fraction

Generally, in ternary compounds, the energy bandgap varies with two solid materials. In the case of  $\text{Cu}_2\text{SnS}_3$ , the energy bandgap varies for Cu and Sn with respect to temperature and doping concentration. Let ‘X’ be the percentage fraction of Cu doping relative to Sn, then  $E_g\text{Cu}_2\text{S}_3$  represents the energy bandgap of copper sulfide,  $E_g\text{SnS}_3$  represents the energy bandgap of tin sulfide and ‘b’ represents the bowing parameter of the  $\text{Cu}_2\text{SnS}_3$  alloy, therefore the energy bandgap of the alloy is represented by equation 1:

$$E_g\text{Cu}_2\text{SnS}_3(X) = XE_g\text{Cu}_2\text{S}_3 + (1 - X)E_g\text{SnS}_3 - bX(1 - X) \quad (1)$$

The bowing parameter ‘b’ is essential for investigating the energy bandgap of ternary alloys [33]. The bowing parameter in semiconductor nanomaterials is described by a parabolic polynomial [34] in equation 2.  $E_g\text{Cu}_2\text{S}_3$  and  $E_g\text{SnS}_3$  are intrinsic bandgaps of initial semiconductors. The degree to which the curve deviates from the linear fit is described by the bowing parameter:

$$b(X) = \frac{XE_g\text{Cu}_2\text{S}_3 + (1 - X)E_g\text{SnS}_3 - E_g\text{Cu}_2\text{SnS}_3(X)}{X(1 - X)} \quad (2)$$

### 2.2. Wavelength analysis by Brus method

L.E. Brus first developed an equation for size dependence of the lowest excited electronic state

for semiconductor nanomaterials under effective mass approximation (EMA). Later, with some modifications, the equation was rearranged as given below. In this approximation, an exciton is considered to be confined to a spherical volume of crystallite. The masses of electron and hole are replaced by an effective mass of electron ( $me^*$ ) and hole ( $mh^*$ ) which are used to define the wave function [35].

$$Eg(Cu_2SnS_3 \text{ QDs}) = Eg(bulk) + h^2/8R^2 \left( \frac{1}{me^*} + \frac{1}{mh^*} \right) - \frac{1.786e^2}{4\pi\epsilon_0\epsilon_r R^2} \quad (3)$$

where  $Eg(QD)$  is the energy band gap of quantum dots,  $Eg(bulk)$  is the energy band gap of bulk semiconductor,  $me^*$  is effective mass of excited electron,  $mh^*$  is effective mass of excited hole,  $R$  is a radius of the quantum dot,  $\epsilon_0$  is permittivity of vacuum,  $\epsilon_r$  is permittivity of concerned semiconductor material,  $h$  is Planck constant and  $e$  is a charge of electron.

The second additive term on the right side of equation 3 is dependent on the inverse of square of the radius of QD, which accounts for the additive energy due to quantum confinement. The third term on right side of equation 3 represents the dielectric constant and is negligible for some nanomaterials [35–37]. Hence, the Brus equation can be rearranged and used as:

$$Eg(Cu_2SnS_3 \text{ QDs}) = Eg(bulk) + h^2/8R^2 \left( \frac{1}{me^*} + \frac{1}{mh^*} \right) \quad (4)$$

In equation 4, by varying the radius ‘ $R$ ’ from 1 nm to 10 nm, the QD wavelength also can be varied. It should be noted that the size of QD confinement region is much smaller than the exciton Bohr radius and comparable to the de Broglie wavelength.

### 2.3. Exciton Bohr radius variation

The exciton Bohr radius  $r_B$  can be calculated from equation 5:

$$r_B = \frac{\epsilon_0\epsilon_r\hbar^2}{e^2} \left( \frac{1}{me^*} + \frac{1}{mh^*} \right) \quad (5)$$

where  $\epsilon_r$  is dielectric constant of material,  $\epsilon_0$  is permittivity of vacuum,  $\hbar$  is reduced Planck constant,  $e$  is charge of carrier.

If the QD radius is larger than the exciton Bohr radius, then the quantum confinement effect will not hold. Therefore, the energy bandgap of such material cannot be calculated by the Brus equation.

## 3. Theoretical parameters for the analysis

The following parameters from the literature have been taken into account for the analysis.

## 4. Results and discussion

The results for bowing parameter ‘ $b$ ’ have been obtained using equation 2. The parameter  $X$  varies from 0.1 to 1.0; the average value of the bowing parameter is 0.34.

By varying the mole fraction of Cu, the possible energy bandgap of  $Cu_2SnS_3$  QDs varies from 1.89 eV for  $X = 0.1$  to 1.21 eV for  $X = 1.0$  (Fig. 3).

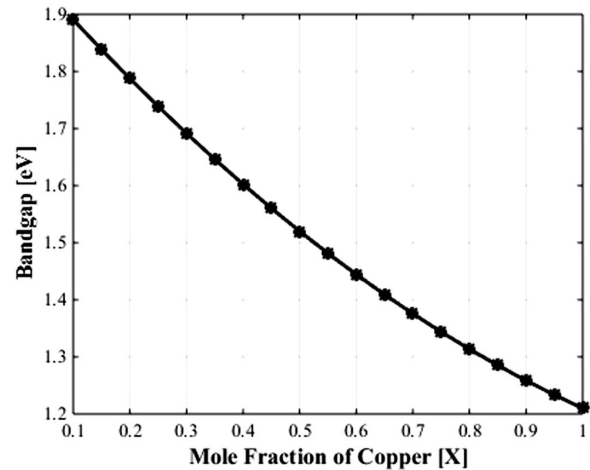


Fig. 3. Change in bandgap of  $Cu_2SnS_3$  with mole fraction of Cu.

As the mole fraction of Cu increases, the energy bandgap of  $Cu_2SnS_3$  tends to decrease to a lower energy bandgap of  $Cu_2S_3$ . The exciton Bohr radius of  $Cu_2SnS_3$  calculated by varying the mole

Table 2. Parameters of different elements.

Parameters	Value	Literature
Energy gap value of ( $\text{Cu}_2\text{SnS}_3$ )	0.9 eV – 1.5 eV	[38]
Effective mass of electron ( $\text{Cu}_2\text{SnS}_3$ )	$2.18 \times 10^{-30}$ kg - $2.73 \times 10^{-30}$ kg	[39]
Effective mass of hole ( $\text{Cu}_2\text{SnS}_3$ )	$1.82 \times 10^{-31}$ kg	[40]
High frequency dielectric constant ( $\text{Cu}_2\text{SnS}_3$ )	$\sim 8.9$	[41]
Energy gap value of ( $\text{Cu}_2\text{S}_3$ )	1.2 eV – 2 eV	[42]
Energy gap value of ( $\text{SnS}_3$ )	2 eV	[43]

fraction of Cu shows that as the mole fraction of Cu increases, the exciton Bohr radius decreases.

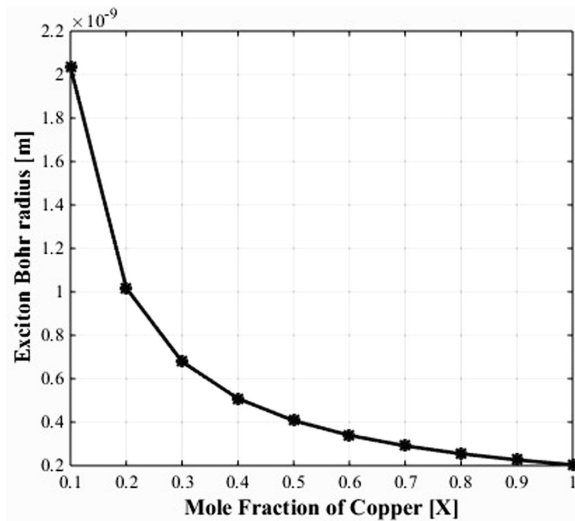


Fig. 4. Exciton Bohr radius variation of  $\text{Cu}_2\text{SnS}_3$  with mole fraction of Cu.

Fig. 4 shows that for  $X = 0.1$  the highest calculated value of exciton Bohr radius is 2.03 nm. Similarly, for  $X = 1$ , the obtained value is 0.2 nm. The range of 0.2 nm to 2.03 nm for the radius of the QDs covers both the wavelengths of visible and near infrared spectrum.

By varying the size of QDs, the optimal energy bandgap can be varied and this helps to find various absorption ranges of frequencies which cover different portions of visible, infrared and near infrared ranges. For radius 'R' with values ranging from 1 nm to 10 nm, the absorption wavelengths ranges from 425 nm to 1348 nm, which covers the visible and infrared ranges.

From Fig. 5 it is observed that, for QDs radius of 1 nm, the absorption wavelength is 425 nm

which lies far from UV spectrum. When the size of QDs radius is slightly increased from 2 nm to 3 nm, the absorption wavelength ranges from visible to near infrared range (688 nm to 881 nm). For fiber optic communication, LEDs and LDs are the sources which provide an input for the fiber to transmit a signal from one place to another. The commercially preferred three ranges of operating wavelength are 850 nm, 1310 nm and 1550 nm. Among these, for short distance communication 850 nm is favored. In  $\text{Cu}_2\text{SnS}_3$  QDs we can easily achieve this wavelength, further, it is observed that it can be tuned to achieve 1310 nm at 6.5 nm radius. Hence, it is highly favorable to fabricate LDs or LEDs for fiber optic communication working under the band ranging from 1260 nm to 1360 nm.

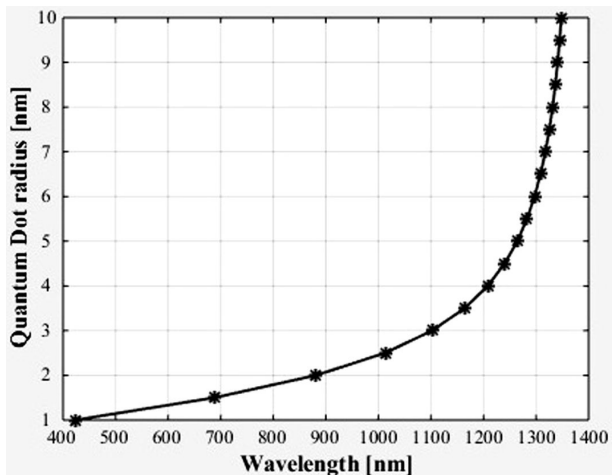


Fig. 5. QDs radius vs. wavelength for  $\text{Cu}_2\text{SnS}_3$  QDs.

It is also observed that, the wavelength is inversely proportional to the energy band gap of material. When energy bandgap is larger,

the wavelength is smaller and the color of light is blue shifted. Similarly, for smaller energy bandgap, the wavelength is larger and the color of light is red shifted. This is very suitable for fabricating LEDs acting as the sources for fiber optic communication. While designing  $\text{Cu}_2\text{SnS}_3$  QDs, the Cu concentration needs to be reduced to provide the low energy bandgap to achieve red shifted QDs.

## 5. Conclusions

$\text{Cu}_2\text{SnS}_3$  QDs have been successfully modeled with respect to tunable energy bandgap, wavelength and mole fraction. The results are as follows.  $\text{Cu}_2\text{SnS}_3$  QDs is a promising candidate for making optoelectronic devices with improved stability. This material can also be used for solar cell applications in single and multilayer band solar cells. Further works is needed for the usage of QDs in optoelectronic sensing devices, whereas in telecommunication devices a little progress in WDMs has been achieved.

## References

- [1] SARGENT E.H., *Adv. Mater.*, 17 (2005), 515.
- [2] JARA D.H., YOON S.J., STAMPLECOSKIE K.G., KAMAT P.V., *Chem. Mater.*, 26 (2014), 7221.
- [3] KO D.K., MAURANO A., SUH S.K., KIM D., HWANG G.W., GROSSMAN J.C., BULOVIC V., BAWENDI M.G., *ACS Nano*, 10 (2016), 3382.
- [4] CHEN J., ZHAO D., LI C., XU F., LEI W., SUN L., NATHAN A., SUN X.W., *Sci. Rep.*, 4 (2014), 4085.
- [5] SONG W.S., YANG H., *Chem. Mater.*, 24 (2012), 1961.
- [6] GONG X., YANG Z., WALTERS G., COMIN R., NING Z.E., BEAUREGAR D., ADINOL V., VOZNY O., SARGENT E.H., *Nat. Photonics*, 10 (2016), 253.
- [7] CHUANG C.H.M., BROWN P.R., BULOVIC V., BAWENDI M.G., *Nat. Mater.*, 13 (2014), 796.
- [8] ZHANG J., GAO J., MILLER E.M., LUTHER J.M., BEARD M.C., *ACS Nano*, 8 (2014), 614.
- [9] CLIFFORD J.P., KONSTANTATOS G., JOHNSTON K.W., HOOGLAND S., LEVINA L., SARGENT E.H., *Nat. Nanotechnol.*, 4 (2009), 40.
- [10] LHUILLIER E., SCARAFAGIO M., HEASE P., NADAL B., AUBIN H., XU X.Z., LEQUEUX N., PATRIARCHE G., ITHURRIA S., DUBERTRET B., *Nano Lett.*, 16 (2016), 1282.
- [11] QIAO K., DENG H., YANG X., DONG D., LI M., HU L., LIU H., SONG H., TANG J., *Nanoscale*, 8 (2016), 7137.
- [12] DABBOUSI B., RODRIGUEZ VIEJO J., MIKULEC F.V., HEINE J., MATTOUSSI H., OBER R., JENSEN K., BAWENDI M., *J. Phys. Chem. B*, 101 (1997), 9463.
- [13] SONG W.S., YANG H., *Chem. Mater.*, 24 (2012), 1961.
- [14] LI L., DAOU T.J., TEXIER I., KIMCHI T.T., LIEM N.Q., REISS P., *Chem. Mater.*, 21 (2009), 2422.
- [15] PARK J., KIM S.W., *J. Mater. Chem.*, 21 (2011), 3745.
- [16] SADIA SULTHANA., SHAH ALAM MD., *IEEE Int. Conf. Comp. Inform. Technol.*, (2015), 550.
- [17] [http://sces.phys.utk.edu/~dagotto/condensed/HW2\\_2009/Quantum\\_Dots.pdf](http://sces.phys.utk.edu/~dagotto/condensed/HW2_2009/Quantum_Dots.pdf), accessed on: 2018.02.08.
- [18] KAMALANATHAN M., HUSSAIN SHAMIMA., GOPALAKRISHNAN R., VISHISTA K., *Mater Technol*, 2 (2017), 1.
- [19] BONK R., BRENOT R., MEUER C., VALLAITIS T., TUSSUPOV A., RODE J.C., SYGLETOS S., VORREAU P., LELARGE F., DUAN G.H., KRIMMEL H.G., PFEIFFER T.H., BIMBERG D., FREUDE W., LEUTHOLD J., *IEEE Int. Conf. Opt. Fiber Commun.*, (2009), 1.
- [20] MICHAL BORECKI., PIOTR DOROZ., PRZEMYSŁAW PRUS., PAWEŁ PSZCZÓLKOWSKI., JAN SZMIDT., MICHAEL L., KORWIN-PAWŁOWSKI., JAROSŁAW FRYDRYCH., ANDRZEJ KOCIUBINSKI., MARIUSZ DUK., *Int. J. Adv. Syst. Meas.*, 7 (2014), 57.
- [21] MIKKELSEN B., DURHUUS T., JORGENSEN C., DANIELSEN S.L., PEDERSEN R.J.S., STUBKJAEER K., *IEEE Proc. Opt. Fiber Commun. Conf.*, (1996), 121.
- [22] RAMAMURTHY BYRAV., MUKHERJEE BISWANATH., *IEEE J. Sel. Areas Commun.*, 7 (1998), 68.
- [23] MEUER C., SCHMIDT-LANGHORST C., BONK R., SCHMECKEBIER H., ARSENIJEVIC D., FIOŁ G., GALPERIN A., LEUTHOLD J., SCHUBERT C., BIMBERG D., *Opt. Express.*, 6 (2011), 5134.
- [24] AKIYAMA T., HATORI N., NAKATA Y., EBE H., SUGAWARA M., *Phys. Status Solidi B*, 2 (2003), 301.
- [25] CONTESTABILE G., MARUTA A., SEKIGUCHI S., MORITO K., KITAYAMA K., *IEEE J. Quantum Electron.*, 4 (2011), 541.
- [26] CONTESTABILE G., MARUTA A., SEKIGUCHI S., MORITO K., KITAYAMA K., *IEEE 35<sup>th</sup> Eur. Conf. Opt. Commun.*, (2009), 1.
- [27] BORECKI M., GECA M., DUK M., KORWIN-PAWŁOWSKI M.L., *J. Elec. Commu. Eng. Res.*, 2 (2017), 1.
- [28] SUGAWARA M., YAMAMOTO T., EBE H., *Fujitsu Sci. Tech. J.*, 4 (2007), 495.
- [29] GIAMPIERO CONTESTABILE., YUKI YOSHIDA., AKIHIRO MARUTA., *IEEE Photon. Technol. Lett.*, 9 (2013), 791.
- [30] KIM H., KWON B.H., SUH M., KANGD.S., KIM Y., JEOND.Y., *Electrochem. Solid State Lett.*, 10 (2011), 55.
- [31] COE-SULLIVAN S., LIU W.Z., ALLEN P., STECKEL J.S., *ECS J. Solid State Sci. Technol.*, 2 (2013), 3026.
- [32] STECKEL J.S., HO J., HAMILTON C., XI J., BREEN C., LIU W., ALLEN P., COE-SULLIVAN S., *J. Soc. Inf. Disp.*, 7 (2015), 294.

- [33] SINEM ERDEN GULEBAGLAN., EMEL KILIT DOGAN., MURAT AYCIBIN., MEHMET NURULLAH SECUK., BAHATTIN ERDINC., HARUN AKKUS., *J. Mod. Phys.*, 5 (2014), 1546.
- [34] SIMA AMINORROAYA YAMINI., VAUGHAN PATTERSON., RAFAEL SANTOS., *ACS Omega*, 2 (2017), 3417.
- [35] BRUS L.E., *J. Chem. Phys.*, 91 (1984), 4403.
- [36] CHUKWUOCHA E.O., ONYEAJU M.C., *Int. J. Sci. Technol. Res.*, 7 (2012), 21.
- [37] CHANGIZ V., ALI E., *Res. J. Recent Sci.*, 1 (2013), 21.
- [38] BARANOWSKI L.L., MCLAUGHLIN K., ZAWADZKI P., LANY S., NORMAN A., HEMPEL H., EICHBERGER R., UNOLD T., TOBERERAND E., ZAKUTAYEV A.S., *Phys. Rev. Appl.*, 4 (2015), 044017.
- [39] SHEN Y., LI C., HUANG R., TIAN R., YE Y., PAN L., KOUMOTO K., ZHANG R., WAN C., WANG Y., *Sci. Rep.*, 6 (2016), 32501.
- [40] ORLETSKII G., SOLOVAN M.N., PINNA F., CICERO G., MARYANCHUK P.D., MAISTRUK E.V., TRESSO E., *Phys. Solid State*, 4 (2017), 801.
- [41] CHEN R., *Doctoral Thesis*, KTH Royal Institute of Technology, 2017.
- [42] FLORES-GARCÍA E., GONZÁLEZ-GARCÍA P., GONZÁLEZ-HERNÁNDEZ J., RAMÍREZ-BON R., *Optik*, 145 (2017), 589.
- [43] KUMAGAI Y., BURTON L., WALSH A., OBA F., *Phys. Rev. Appl.*, 6 (2016), 014009.

Received 2018-02-09  
Accepted 2018-05-26